Auxiliary material for

Holocene slip rate along the Gyaring Co fault, central Tibet

Xuhua Shi[1*], Eric Kirby[2], Haijian Lu[3], Ruth Robinson[4], Kevin Furlong[1], Erchie Wang[5]

1. Department of Geosciences, Pennsylvania State University, University Park, PA 16802, USA
2. College of Earth, Ocean, and Atmospheric Sciences, Oregon State University, Corvallis, OR, USA
3. Institute of Geology, Chinese Academy of Geological Sciences, Baiwanzhuang Road, Beijing 100037, China
4. Department of Earth and Environmental Sciences, University of St Andrews, St Andrews KY16 9AL, Scotland, UK
5. Institute of Geology and Geophysics, Chinese Academy of Sciences, Beijing 100029, CHINA

Geophysical Research Letters

Introduction

This auxiliary material includes two sections labeled as S1 and S2 that describe the field sampling (labeled as S1) and laboratory processing (labeled as S2) of optically stimulated luminescence (OSL) samples for dating the shoreline deposits. The laboratory processing of OSL samples contains three sections: 1) sample preparation, 2) luminescence measurements, and 3) environmental dose determination. Also contained here are figures and tables related to the auxiliary text and the main manuscript.

S1. Field sampling of OSL samples

Given that no stream-cut stratigraphy was found in these highstand shorelines, depth profile pits (> 0.5 m – 2.5 m deep) have been dug to observe a limited dimension of vertical and lateral stratigraphy. All samples were carefully collected from sand layers/lenses that are intercalated within the upper beach gravel deposits (Figure S1 and S2) that can reflect ages of the most recent highstand shorelines hence lake levels. Eolian sands (younger than the age of shoreline deposition) at the top of the shoreline stratigraphy are definitely avoided. Before collecting the sand samples, the light-affected surface deposits of several centimeters thick were removed to reduce the uncertainty from dose measurement [*Aitken*, 1998]. Sands of medium, fine or silt sizes were drilled using plastic PVC (Polyvinyl chloride) and or steel tubes, 3 cm or 5 cm in diameter, depending on the consolidation and thickness of the sand layers. These tubes were then wrapped with heavy duty black duct tape to avoid light penetration and keep the water content.

S2. Laboratory processing of OSL samples

S2.1 Sample preparation

Samples were prepared using standard OSL procedures. Material was desiccated at 50 ˚C to enable calculation of water content, and then sieved to extract the 180-212 µm grain size fraction. Approximately 10 g of the 180-212 µm grain size fraction was treated with 30% HCl for 30 minutes to remove CaCO3. Samples were agitated throughout the treatment, and once complete, HCl was replaced with 30% H_2O_2 to remove organic material. The duration of H_2O_2 treatment varied between samples, dependent upon the amount of organic material present. Once effervescence ceased, the H_2O_2 was decanted, the sample was washed four times with deionised water and desiccated at 50 ˚C. Quartz is extracted from polymineral sediment residues through density separations using LST fastfloat (sodium heteropolytungstate dissolved in deionized water). Heavy minerals (> 2.68 g cm^{-3}) were separated from the lighter fraction, and the target 2.58-2.68 gcm^{-3} fraction was further separated from the < 2.58 g cm^{-3} material. The target fraction was washed five times with deionised water to ensure removal of all LST. Final separates were dried and etched with 40% HF for 40 minutes to remove any contaminating feldspar; all samples were agitated at 5 minute intervals throughout treatment. The etched quartz was treated with 30% HCl for 30 minutes to remove any carbonates produced during HF etching.

S2.2 Luminescence measurements

All analyses were carried out using either a TL-DA-15 [*Bøtter-Jensen et al.*, 2003] or TL-DA-20 Risø reader, equipped with an EMI 9235QA photomultiplier and 7.5 mm Hoya U-340 filter. Blue (470±20 nm) and infrared (~870 nm) diodes operated at 90% and

40% power respectively, were used for stimulation and irradiation was achieved using a 90Sr/90Y beta source. Readers were calibrated using quartz prepared at the Risø National Laboratory in Denmark. Quartz was applied to stainless steel discs (10 mm Ø, 1 mm thick) using silicon grease and the aliquot size was regulated using a small (2 mm Ø, ~35 grain) mask.

Samples were analysed using the single aliquot regenerative dose (SAR) protocol [*Murray and Wintle*, 2000]. The equivalent dose (De) was calculated from measurements of the luminescence response following stimulation of the natural luminescence (Ln) and a series of different regenerative doses (Lx). The Ln and Lx measurements are normalised by measurement of the luminescence response (Tx) to a constant test dose (TD). The ratio Lx/Tx is used to compensate for sensitivity changes of the quartz throughout analysis and Lx/Tx measurements are used to obtain a range of values which bracket Ln/Tx, allowing De interpolation with minimal associated errors [*Banerjee et al.*, 2000].

The sample is heated prior to making the luminescence measurements in order to reduce the contribution of luminescence from unstable trap, which cause erroneous dose determinations. The temperature of the pre-Lx pre-heat (PH1) and the pre-Tx pre-heat (PH2) must be empirically determined for each sample under analysis. This was achieved through analysis of 8 disks with a dose-recovery pre-heat plateau experiment [*Murray and Wintle*, 2003], using a range of PH1 and PH2 temperatures ranging from 150 – 220 ^{o}C. The influence of a hot-bleach at 280 °C was also investigated [*Murray and Wintle*, 2003] but was not required to counter any thermal transfer or recuperation.

The SAR protocol with a PH1 of 200 °C used on most of the samples is provided in Table S1. Aliquot acceptance criteria used are 1) recycling ratios within 10% of unity; 2) signal intensities ≥ 3 σ above background; 3) infra-red (IR) depletion ratio within 20% of unity [*Duller,* 2003]; 4) De uncertainty ≤ 20 % and 5) recuperation within 10% of the normalised maximum dose. The acceptance thresholds are generally very high for the samples (85 – 100%) reflecting the sensitivity of the quartz analysed. All three samples have at least 50 accepted aliquots.

S2.3 Environmental Dose rate determination

The environmental dose rates (Dr) were calculated for each sample from the unsieved portions of the original sample; concentrations of U, Th, K and Rb were measured directly using solution ICP-MS (Thermo X-Series), a cosmic-dose component after *Prescott and Hutton* [1994] and an internal alpha dose rate of 5% from the decay of U and Th after *Sutton and Zimmerman* [1978]. External α-dose rates were ignored as the alpha irradiated portion of quartz grains was removed by etching. The conversion factors of *Adamiec and Aitken* [1998] and beta-particle attenuation factors after *Mejdahl* [1979] and *Readhead* [2002a]; [2002b] have been used. Sample water content was calculated following desiccation at 50 °C, and an uncertainty of 5 % assumed. Tables S2 and S3 contain the dosimetry and age data of OSL samples from the highstand shorelines.

S2.4 Analysis of OSL ages

All three samples are characterized by large overdispersion values (broad distributions of equivalent dose, see Figure 4 in the main document and Figure S6) [*Galbraith et al.,* 1999] of 21-23%; samples with overdispersion greater than 20% are typically assumed to reflect heterogeneous bleaching before deposition. An age model

was selected for each sample following the criteria of *Arnold and Roberts* [2009]. Two of the samples (GR2 and GR3) are modelled using the three component minimum age model (MAM-3) and one sample (GR1) is based on a central age model (CAM) [*Galbraith et al.*, 1999] using the RStudio Luminescence package [*Kreutzer et al.*, 2012].

Supplemental References

Adamiec, G., and M. Aitken (1998), Dose-rate conversion factors: update, *Ancient tL*, *16*(2), 37-50.

Aitken, M. J. (1998), *An introduction to optical dating: The dating of Quaternary sediments by the use of photon-stimulated luminescence*, 280 pp., Oxford University Press.

Arnold, L. J., and R. G. Roberts (2009), Stochastic modelling of multi-grain equivalent dose (De) distributions: Implications for OSL dating of sediment mixtures, *Quaternary Geochronology*, *4*(3), 204-230, doi: 10.1016/j.quageo.2008.12.001.

Banerjee, D., L. Botter-Jensen, and A. S. Murray (2000), Retrospective dosimetry: estimation of the dose to quartz using the single-aliquot regenerative-dose protocol, *Applied Radiation and Isotopes*, *52*(4), 831-844.

Bøtter-Jensen, L., S. W. S. McKeever , and A. G. Wintle (2003), *Optically Stimulated Luminescence Dosimetry*, 355 pp., Elsevier Science, Amsterdam.

Duller, G. A. T. (2003), Distinguishing quartz and feldspar in single grain luminescence measurements, *Radiation Measurements*, *37*(2), 161-165.

Galbraith, R. F., R. G. Roberts, G. Laslett, H. Yoshida, and J. M. Olley (1999), Optical dating of single and multiple grains of quartz from jinmium rock shelter, northern australia: part i, experimental design and statistical models*, *Archaeometry*, *41*(2), 339-364.

Kreutzer, S., C. Schmidt, M. C. Fuchs, M. Dietze, M. Fischer, and M. Fuchs (2012), Introducing an R package for luminescence dating analysis, *Ancient TL*, *30*(1), 1-8.

Mejdahl, V. (1979), *Thermoluminescence Dating: Beta-Dose Attenuation in Quartz Grains*.

Murray, A. S., and A. G. Wintle (2000), Luminescence dating of quartz using an improved single-aliquot regenerative-dose protocol, *Radiation Measurements*, *32*(1), 57-73.

Murray, A. S., and A. G. Wintle (2003), The single aliquot regenerative dose protocol: potential for improvements in reliability, *Radiation Measurements*, *37*(4-5), 377-381.

Prescott, J. R., and J. T. Hutton (1994), Cosmic ray contributions to dose rates for luminescence and ESR dating: Large depths and long-term time variations, *Radiation Measurements*, *23*(2-3), 497-500.

Readhead, M. L. (2002a), Absorbed dose fraction for ^{87}Rb β particles, *Ancient TL*, *20*(1), 25-28.

Readhead, M. L. (2002b), Addendum to "Absorbed dose fraction for ^{87}Rb β particles", *Ancient TL*, *20*(2), 47.

Sutton, S. R., and D. W. Zimmerman (1978), Thermoluminescence dating: radioactivity in quartz, *Archaeometry*, *20*, 66-88.

Supplemental Table Captions

Table S1. Quartz SAR protocol for all Tibet samples.

Table S2. OSL sample locations and age calculation data of the displaced shorelines along the Gyaring Co fault.

Table S3. Chemical data of OSL samples of the displaced shorelines along the Gyaring Co fault.

Supplemental Figure Captions

Figure S1. Example photos showing the depositional setting of sample GR1 in the G3 highstand shoreline along the SE margin of Zigui Co. (a) The surface of the beach ridge. (b) The depth profile showing a thin layer of medium-grained sands interbedded within beach gravel layers above and below. (c) Detailed view of the sample layer.

Figure S2. Example photos showing the depositional setting of sample GR2 in the G3 highsand shoreline along the SE margin of Zigui Co. (a) The depth profile showing a thin layer with mixture of medium-grained sands and beach gravels that is interbedded within beach gravel layers above and below.

Figure S3. Example photos showing the depositional setting of sample GR3 in the eolian sands deposited in the back-ridge depression of the G3 highstand shoreline along the SE margin of Zigui Co. (a) The photo (looking to the east) that shows an overview of the

topography of the S1 beach ridge. (b) The intermediate view of the sample site. (c) Detailed view of the fine-grained sand sample.

Figure S4. (a) GeoEye imagery showing shoreline groups G2, G3 and G4 at the southeastern margin of Zigui Co where the G3 highstand shorelines were displaced. The bracket south of the fault represents the straight parts of the shorelines (~ 350 – 400 m), the center lines of which are used to reconstructed the fault offset across the shorelines. (b) The field photo (looking to the south) that shows the fault offset across the G3 highstand shoreline (see location in panel A). (c) The field photo (looking to the south) that shows the cross-section of the S1 beach ridge of the G3 highstand shorelines. A narrow flat ridge crest (~ 1 m wide) can be clearly seen from this photo.

Figure S5. GeoEye imagery (left) and sketch (right) showing the displaced old alluvial terraces (T2-T4) and also the undisplaced youngest terrace (T1). Red lines show the fault traces and hatched polygons represent the terrace risers.

Figure S6. (a-c) The density function and cumulative frequency of equivalent dose (De) for OSL samples GR-1, 2, and 3, respectively.

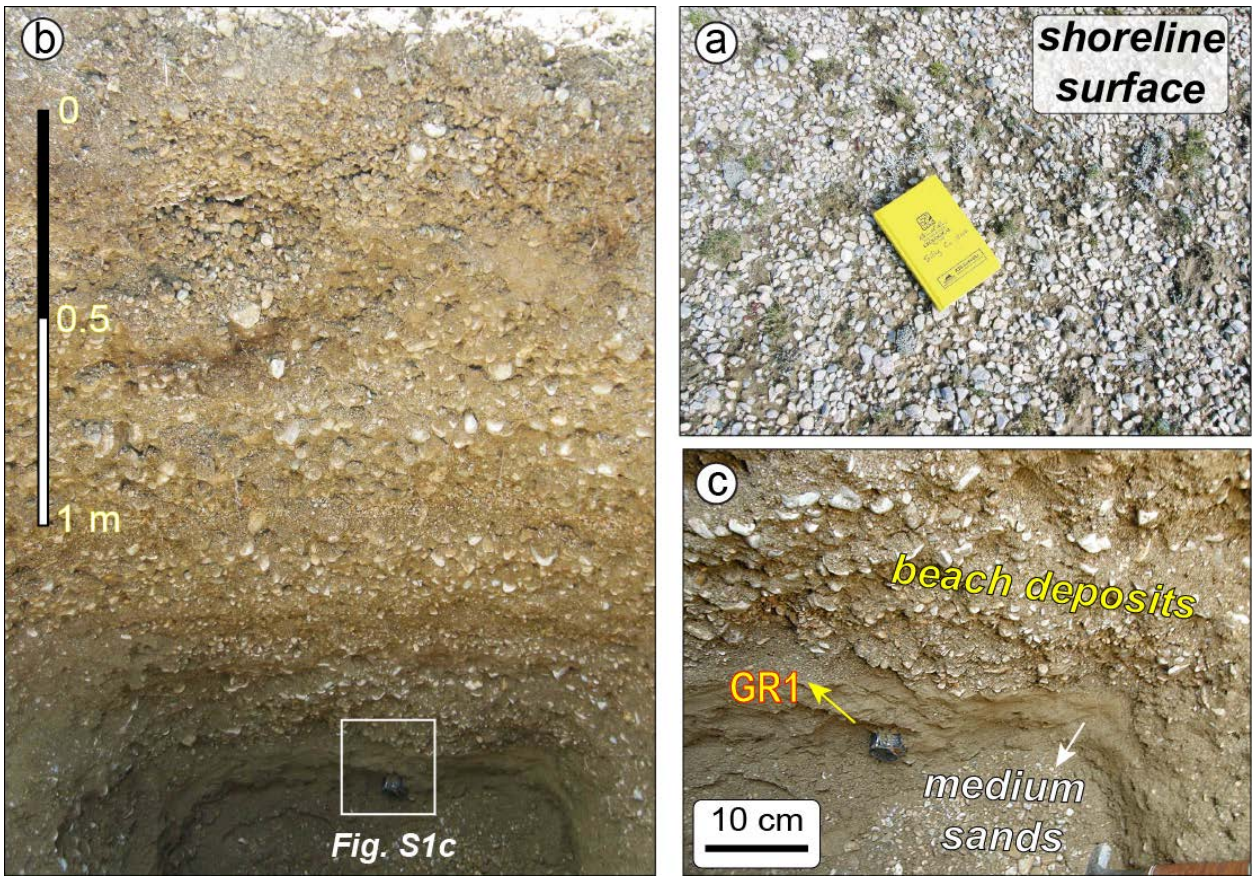
b
0
0.5
1 m
Fig. S1c
a
shoreline surface
c
beach deposits
GR1
medium sands
10 cm

Figure S1

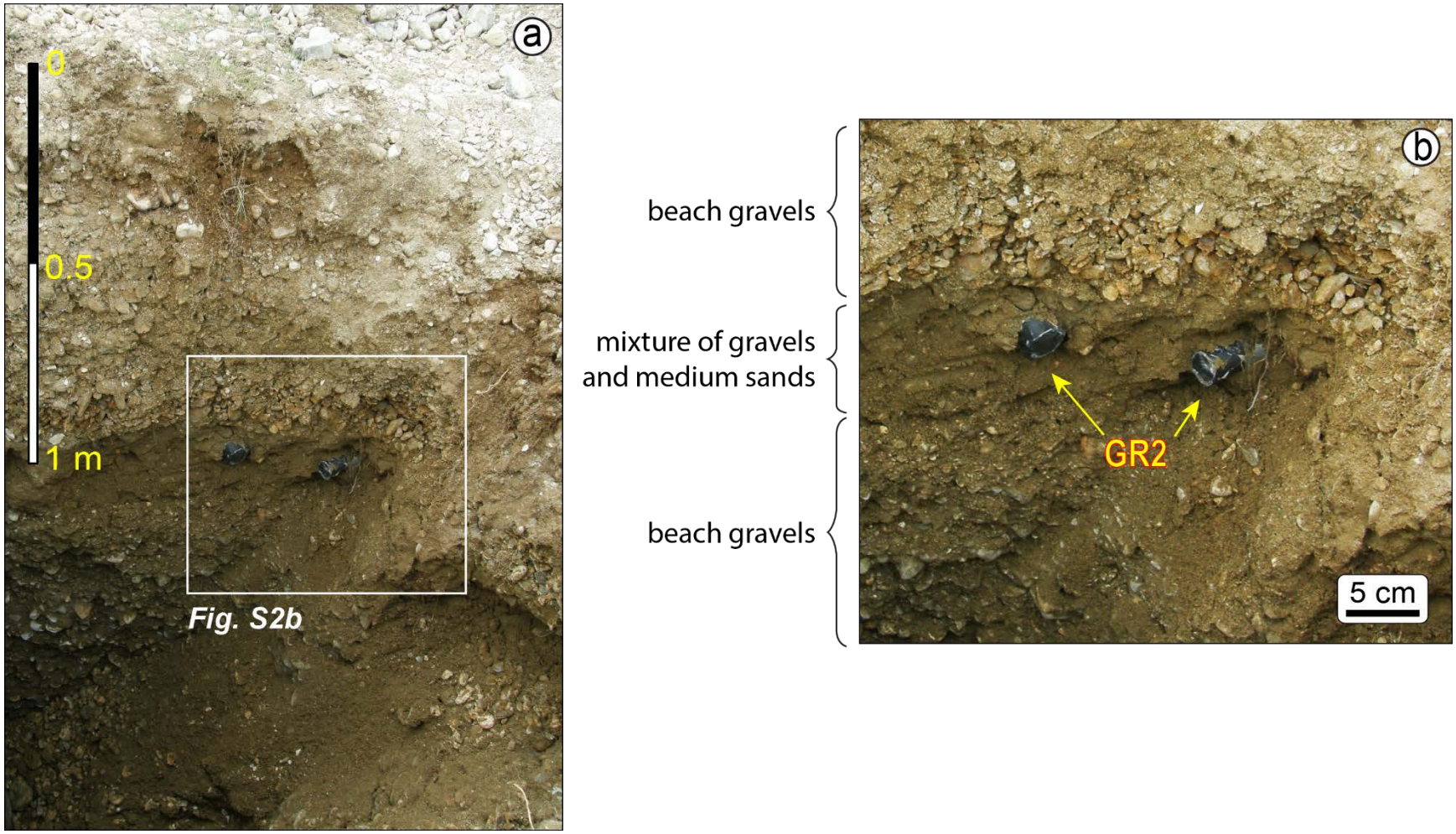
a
0
0.5
1 m
Fig. S2b
beach gravels
mixture of gravels
and medium sands
beach gravels
b
GR2
5 cm

Figure S2

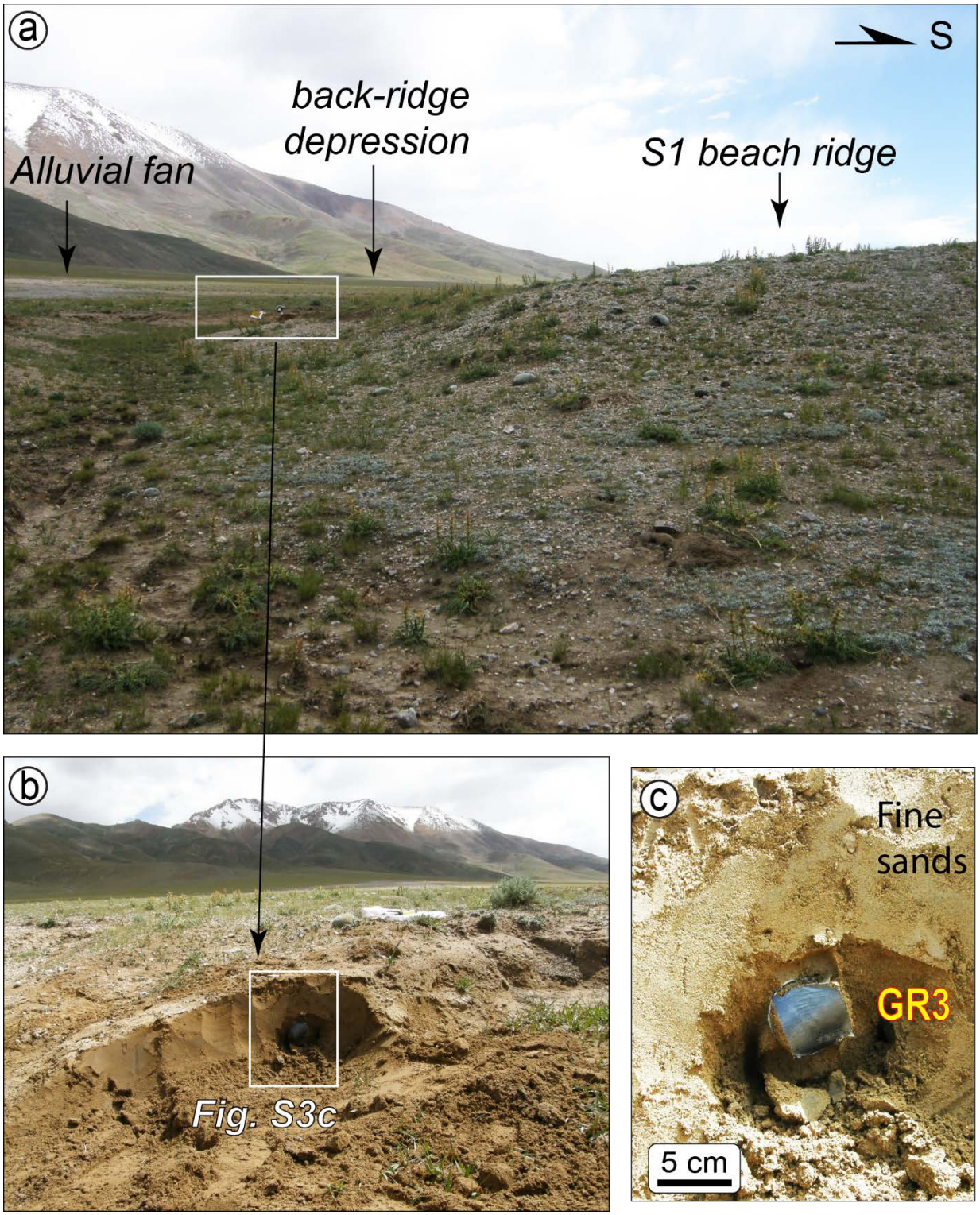
a
S
back-ridge
depression
Alluvial fan
S1 beach ridge
b
Fig. S3c
c
Fine
sands
GR3
5 cm

Figure S3

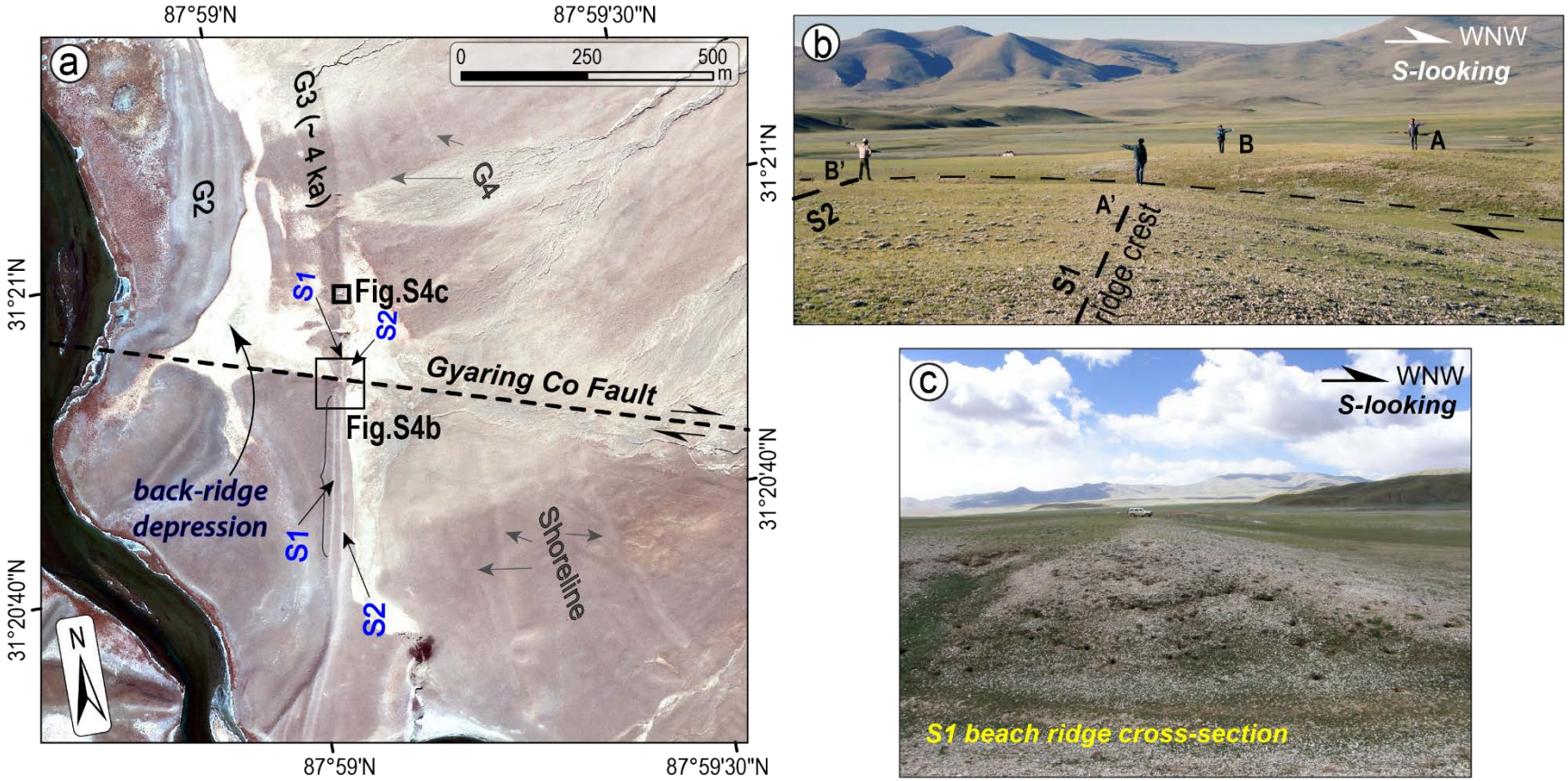
a
87°59'N
87°59'30"N
31°21'N
31°20'40"N
0
250
500
m
G3 (~ 4 ka)
G4
G2
S1
Fig.S4c
S2
Gyaring Co Fault
Fig.S4b
back-ridge
depression
S1
S2
Shoreline
N
b
WNW
S-looking
B
A
B'
A'
S2
S1
ridge crest
c
WNW
S-looking
S1 beach ridge cross-section

Figure S4

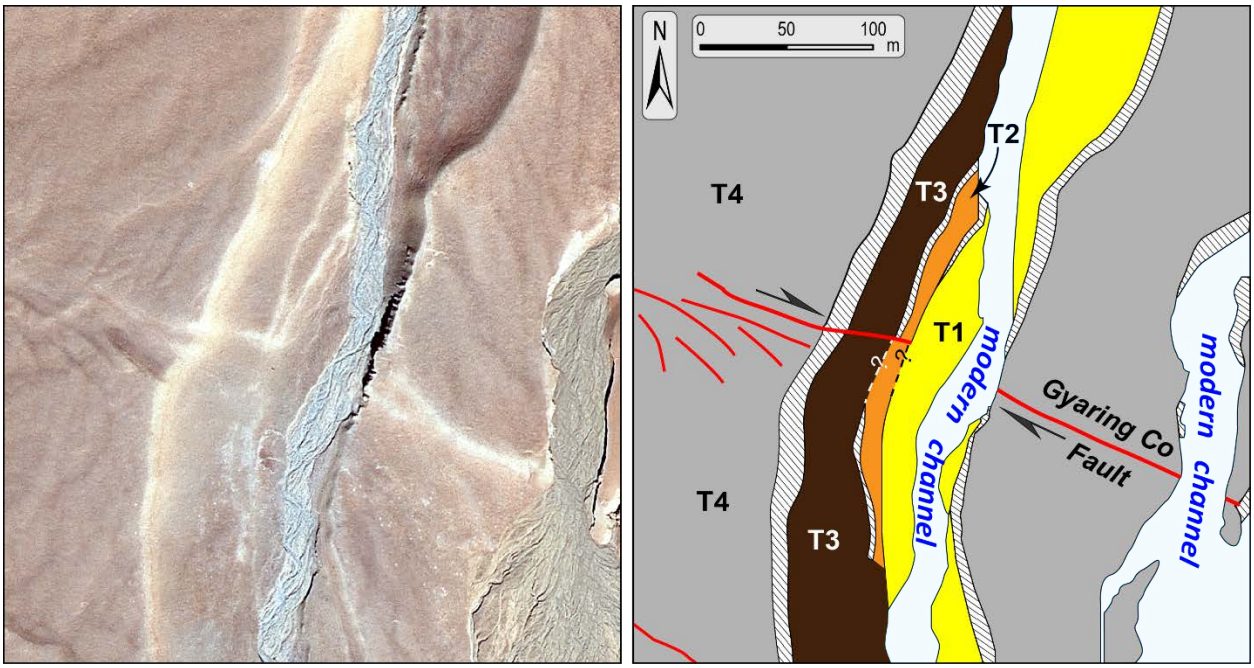
N
0
50
100
m
T4
T3
T2
T1
T4
T3
modern channel
Gyaring Co
Fault
modern channel

Figure S5

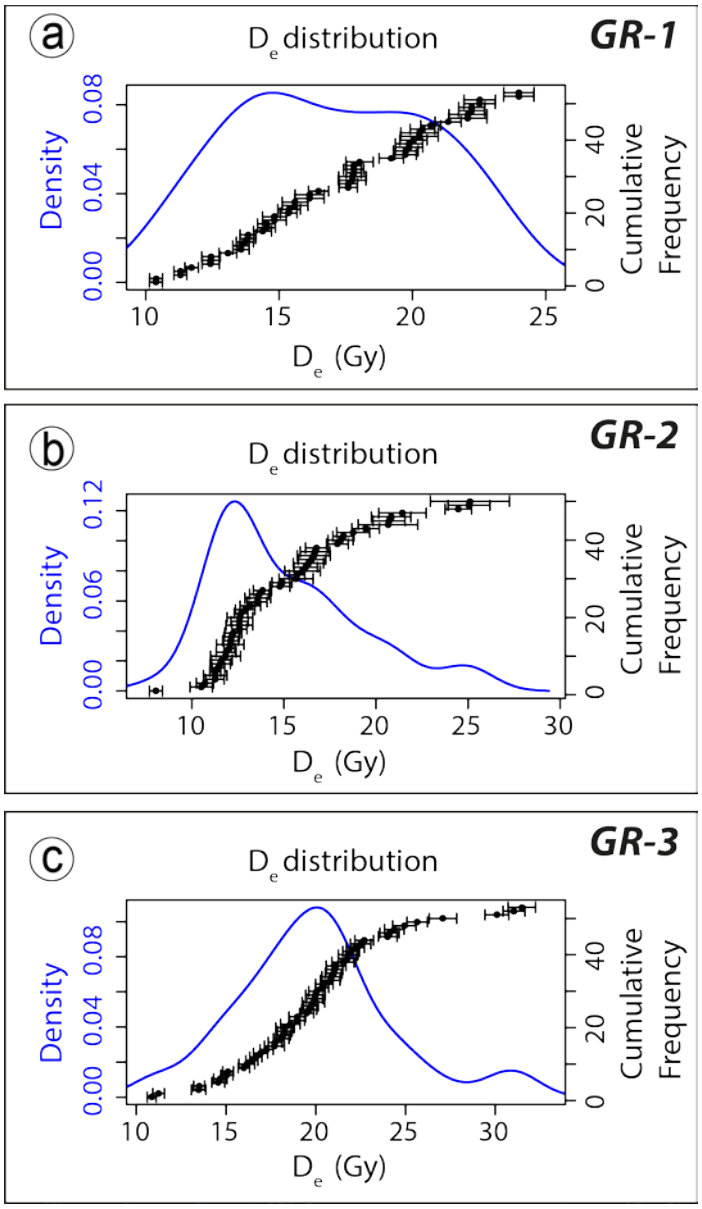
a
D$_e$ distribution
GR-1
Density
0.00
0.04
0.08
Cumulative Frequency
0
20
40
10
15
20
25
D$_e$ (Gy)
b
D$_e$ distribution
GR-2
Density
0.00
0.06
0.12
Cumulative Frequency
0
20
40
10
15
20
25
30
D$_e$ (Gy)
c
D$_e$ distribution
GR-3
Density
0.00
0.04
0.08
Cumulative Frequency
0
20
40
10
15
20
25
30
D$_e$ (Gy)

Figure S6

Table S1: Quartz SAR protocol for all Tibet samples

Natural/Regenerative Dose	5, 10, 20, 30, 0, 5, 5 Gy
TL (PH1)	200˚C, 10 s, 5˚C/s
IRSL (final cycle only)	20˚C, 40 s, 5˚C/s
OSL	125˚C, 40 s, 5˚C/s, 90% power (*Lx*)
Test Dose	5 Gy
TH (PH2)	180˚C, 10 s, 5˚C/s
OSL	125˚C, 40 s, 5˚C/s, 90% (*Tx*)

Table S2. **OSL sample locations and age calculation data of the displaced shorelines along the Gyaring Co fault.**

Sample ID	Lat (°N)	Long (°E)	Elev. (m)	Samp_Depth (m)	N (aliquots)	De (Gy)	Error (Gy)	Dose Rate (Gy/kyr)	Error (Gy/kyr)	Age (ka BP)	Uncert_2σ (ka)	Age Model
GR1	31.347	87.985	~ 4665	1.8	53	16.6	0.5	4.1	0.1	4.1	0.1	CAM
GR2	31.347	87.985	~ 4665	1.1	50	11.6	0.7	2.8	0.1	4.1	0.3	MAM-3
GR3	31.350	87.985	~ 4665	0.15	53	15.9	0.9	3.6	0.1	4.4	0.3	MAM-3

* MAM – Minimum age model; CAM – central age model; numbers denote the component of each age model

Table S3. Chemical data of OSL samples of the displaced shorelines along the Gyaring Co fault.

Sample ID	U (ppm)	Error (ppm)	Th (ppm)	Error (ppm)	K (%)	Error (%)	Rb (ppm)	Error (ppm)	H_2O (wt. %)	Error (wt. %)	Cosmic ($mGya^{-1}$)	Error (10%)
GR1	2.90	0.09	12.90	0.39	2.37	0.07	139.20	13.92	6.73	0.34	0.43	0.04
GR2	2.30	0.07	9.30	0.28	1.35	0.04	91.30	9.13	5.50	0.28	0.47	0.05
GR3	2.90	0.09	11.10	0.33	2.01	0.06	125.00	12.50	9.43	0.47	0.54	0.05